Velocity-space tomography using prior information at MAST

B. Madsen,[1, a)] M. Salewski,[1] J. Huang,[2] A. S. Jacobsen,[3] O. Jones,[4] K. G. McClements,[4] and the MAST team[4]

[1)] *Department of Physics, Technical University of Denmark, Kgs. Lyngby, Denmark*
[2)] *Institute of Plasma Physics, Chinese Academy of Sciences, P.O. 1126, 230031 Hefei, Anhui, China*
[3)] *Max-Planck-Institut für Plasmaphysik, Garching, Germany*
[4)] *CCFE, Culham Science Centre, Abingdon, Oxfordshire OX14 3DB, UK*

Velocity-space tomography provides a way of diagnosing fast ions in a fusion plasma by combining measurements from multiple instruments. We use a toroidally viewing and a vertically viewing fast-ion D-alpha (FIDA) diagnostic installed on the spherical tokamak MAST (before the upgrade) to perform velocity-space tomography of the fast-ion distribution function. To make up for the scarce amount of data, prior information is included in the inversions. We impose a non-negativity constraint, suppress the distribution in the velocity-space region associated with null-measurements, and encode the belief that the distribution function does not extend to energies significantly higher than those expected neoclassically. This allows us to study the fast-ion velocity distributions and the derived fast-ion densities before and after a sawtooth crash.

I. INTRODUCTION

It is crucial to study the behaviour and confinement of energetic ions since they are essential to heat the plasma and, in fusion reactors, might damage the first wall if they escape the plasma[1]. In deuterium plasmas, one method of doing so is by fast-ion D-alpha (FIDA) spectroscopy[2,3] which has been implemented in numerous tokamaks and stellarators around the world[3–9]. FIDA measures the Balmer-alpha radiation from a neutralized fast ion following a charge-exchange reaction. The neutrals donating the electron are mostly those injected into the plasma by neutral beam injection (NBI). The spatial measurement volumes of the FIDA views are thus defined by the overlap between the lines-of-sight and the neutral beam. In the mega-amp spherical tokamak (MAST), toroidally and vertically directed FIDA views were installed[9,10]. We combine measurements from this dual-view FIDA system on MAST in reconstructions of the fast-ion distribution function before and after a sawtooth crash providing essential information about the resulting fast-ion density decrease. Similar investigations have been carried out at ASDEX Upgrade[7,11–13]. The tomography problem based on FIDA measurements at MAST is a scarce-data problem, and parts of velocity-space are covered by only one view. Therefore, tomographic inversion methods[13] used for the reconstruction of the fast-ion velocity distribution from FIDA measurements at ASDEX Upgrade are here plagued by severe artifacts. To make up for the scarce amount of data, we include the outer shape of the neoclassically expected distribution as a new type of prior information in the tomographic inversions. This enables the reconstruction of the fast-ion velocity distribution before and after a sawtooth crash.

The paper is organized as follows. Sec. II introduces the modelled and experimental signals. The data analysis methods are described in Sec. III, whilst Sec. IV
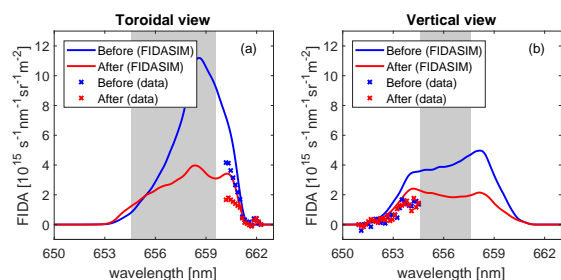
a)birma@fysik.dtu.dk

FIG. 1. Central measurements and FIDASIM simulations of the toroidal (a) and vertical (b) views before and after the sawtooth crash. The shaded areas mark the regions where the beam or thermal-ion emissions dominate the FIDA signal.

illustrates the methods on synthetic data. This is used to reconstruct the fast-ion velocity-space distribution before and after a sawtooth crash in Sec. V. Sec. VI concludes the paper.

II. MODELLED AND EXPERIMENTAL SIGNALS

MAST[14] is a low aspect ratio $R/a \approx 1.3$ tokamak with major radius $R \approx 0.85$ m and minor radius $a \approx 0.65$ m. We study the fast-ion distribution before ($t = 0.253$ s) and after ($t = 0.279$ s) a sawtooth crash observed by the dual-view FIDA diagnostics with lines-of-sight intersecting the SS NBI beam at $r = 1.13$ m during shot #29881.

The expected signals for each view before and after the sawtooth crash are modelled with FIDASIM[15] based on TRANSP simulations (Figure 3) in which fast ions are modelled in NUBEAM[16]. The predicted FIDA spectra and the measurements are plotted in Figure 1. At low Doppler-shifts from the D-alpha emission line at 656.1 nm, the FIDA signal is masked by the much stronger thermal D-alpha and beam emissions. This is illustrated by shaded areas in Figure 1. Therefore only the wings of the spectra are accessible. For the toroidal and vertical views, FIDA measurements are accessible in the ranges between $[660.2 - 662.25]$ nm and
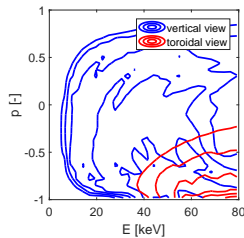
FIG. 2. (E, p)-space interrogation regions related to the experimentally accessible wavelength ranges in the toroidal ($[660.2 - 662.25]$ nm) and vertical ($[650.96 - 654.5]$ nm) views.

$[650.96 - 654.5]$ nm, respectively.

The measured signal in a given wavelength range relates to regions in velocity-space through so-called fast-ion weight functions[17]. The weight function depends on the observed wavelength range and the viewing angle ϕ between the line-of-sight and local magnetic field in the measurement volume. Hence the toroidal ($\phi_t = 36°$) and vertical ($\phi_v = 104°$) views are sensitive to different regions in velocity-space.

Figure 2 depicts the total interrogation regions related to the experimentally accessible wavelength domains for the toroidal and vertical views. These are shown in the widely used energy $E = \frac{1}{2}m_D v^2$ and pitch $p = v_{||}/v$ space where v is the fast-ion speed and $v_{||}$ is its velocity component along the magnetic field. From this it is evident that the accessible part of the spectra from the toroidal view is sensitive to high energies ($\sim 40 - 80$ keV) at negative pitches, whilst observations from the vertical view are sensitive to much lower energies in a broader pitch-range. Since the beam injection direction in MAST is counter to the toroidal field, most of the beam ions have negative pitches.

III. INVERSION METHODS USING PRIOR INFORMATION

Fast-ion velocity-space tomography is based on finding the solution F^* to the mathematically ill-posed problem

$$WF^* = S \qquad (1)$$

where W is the transfer matrix containing the weight functions and S is the measured signal[18,19]. W and S are normalized by the measurement uncertainty[20]. In order to find a stable solution, first-order Tikhonov regularization[21] has proven a useful tool in tomography studies[7,12,13,22,23]. Here the solution is regularized by introducing a penalty term that favours solutions with small gradients. The solution F^* is then the distribution F that minimizes the sum of the residual norm of the original problem (Eq. 1) and the norm of the regularization of the solution. This can be written as

$$F^* = \arg\min_F \left\| \begin{pmatrix} W \\ \lambda_1 L_1 \end{pmatrix} F - \begin{pmatrix} S \\ 0 \end{pmatrix} \right\|_2 \qquad (2)$$
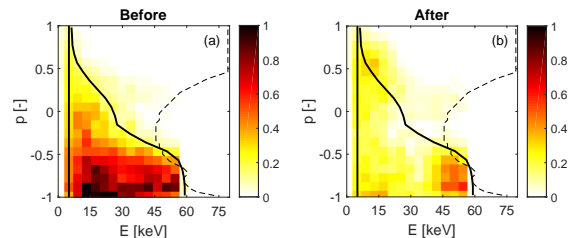

FIG. 3. TRANSP simulation of the fast-ion distribution in (E, p)-space at $r = 1.13$ m, before (a) and after (b) the sawtooth crash. The vertical black line indicates the lower limit of the velocity-space, we seek to reconstruct. The curved black line is the lower limit of the unlikely velocity-space region. The null-measurement region lies to the right of the dashed line. The same normalisation factor is used for both plot.

where L_1 is the gradient matrix[12], and λ_1 is the regularization parameter. Here, the indices refer to the order of the Tikhonov regularization. The regularization parameter determines the strength of the regularization and is, in Sec. IV, chosen such that the solution error is minimized.

To improve the solution, additional prior-information can be included in so-called high-definition tomography. High-definition velocity-space tomographies of fast ions in fusion plasmas have included non-negativity, null-measurements, known peak-locations, and numerical simulations[13] as prior information. Specifically, studies have shown that adding the non-negativity constraint, i.e. $F^* \geq 0$, improves the reconstruction[7,13]. Therefore, this is used throughout this study.

A. Null-measurements as a hard constraint

Including null-measurements as a hard constraint in the reconstructions sets the solution to zero in specific parts of velocity-space based on spectral observations. Null-measurements are the parts of the spectra where the observed light is consistent with the absence of FIDA light[13]. In Figure 1, the null-measurements are above 661.48 nm in the toroidal view and below 651.4 nm in the vertical view. The associated velocity-space is to the right of the dashed curved lines in Figure 3, which agrees well with scarcely populated regions in the neoclassical simulations by TRANSP both before and after the sawtooth crash.

Previously, null-measurements have been implemented by constraining the solution to be zero at the coordinates (E_0, p_0) in the regions covered by null-measurements, i.e. $F(E_0, p_0) = 0$. Therefore with this and non-negativity,
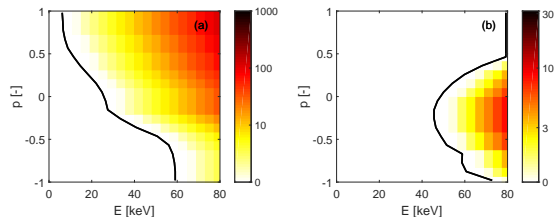
FIG. 4. Exponentially growing penalty function ξ above what is neoclassically expected by the TRANSP simulation (a) and in the null-measurement region (b).

the solution becomes

$$F^* = \arg\min_F \left\| \begin{pmatrix} W \\ \lambda_1 L_1 \end{pmatrix} F - \begin{pmatrix} S \\ 0 \end{pmatrix} \right\|_2$$
$$\text{subject to } \begin{cases} F^* \geq 0 \\ F^*(E_0, p_0) = 0 \end{cases}. \quad (3)$$

This method removes artifacts in the null-measurement region. However, it might introduce artifacts at the sharp boundary between the tomography and null-measurement region. A second concern is that the hard constraint makes it impossible to detect any ions in the null-measurement region[13]. Our new approach presented in the next section overcomes these limitations by changing the hard constraint to a penalty.

B. Unlikely velocity-space due to null-measurements and due to neoclassical simulations

Since it is only highly unlikely to have an ion in e.g. the null-measurement region but not strictly impossible, we propose to penalize the solution with increased penalty strength further into the region instead of forcing the solution to zero herein. We refer to the region where the presence of ions is unlikely as the unlikely velocity-space. The penalty allows fast ions in this region, but still suppresses clear artifacts. In addition, the smooth nature of the penalty function removes the sharp boundary into the unlikely velocity-space often appearing in tomographies using the hard constraint.

The unlikely velocity-space method is implemented by introducing an additional penalty term in the Tikhonov problem of Eq. (2). This term penalizes solution norms in the unlikely velocity-space, but does not penalize the solution outside this region. This is encoded in the function $\xi = \xi(E, p)$ that is multiplied onto the zeroth-order Tikhonov penalty operator L_0 which is the identity matrix.

The strength of the penalty is determined by the regularization parameter λ_0 chosen to be as low as possible but still strong enough to suppress clear artifacts in the unlikely velocity-space. This can be determined by inversions of synthetic measurements where the true solution is known such that artifacts can be identified. In

order to improve the reconstruction, the solution is still sought to be smooth over the entire domain. Together with the non-negativity constraint, the solution of the unlikely velocity-space method takes the form

$$F^* = \arg\min_F \left\| \begin{pmatrix} W \\ \lambda_1 L_1 \\ \lambda_0 \xi L_0 \end{pmatrix} F - \begin{pmatrix} S \\ 0 \\ 0 \end{pmatrix} \right\|_2$$
$$\text{subject to } F^* \geq 0. \quad (4)$$

We use this method on both the null-measurement region and in the region where the TRANSP simulation suggests marginal fast-ion densities far below the detection limit of the diagnostic. For NBI populations there is usually a fairly sharp transition between densely and scarcely populated velocity-space regions (see Figure 3), so that these regions can be separated. We then assume that the larger the distance from the separation line in Figure 3 within the unlikely velocity-space, the lower the likelihood of finding ions. Here the penalty function ξ is chosen to increase exponentially with increased energy and takes the forms shown in Figure 4.

Even though this method does not force the solution to zero in the unlikely velocity-space, the solution will be more strongly suppressed in this region. Therefore, this method must be used with care on real experimental data where the true solution is not known, and features removed from the less-constrained solutions by this method must be deemed artifacts before being suppressed. This is especially true when assuming only a low likelihood of ions above the TRANSP upper boundary, where the imposed unlikely velocity-space is not deduced from the measurements but rather from neoclassical simulations. However, the purpose of this study is not to verify the simulation shape from experimental measurements. Instead we wish to improve the tomographic reconstructions of fast-ion distributions from two-view FIDA measurements in MAST where the non-negativity and hard null-measurement constraints turn out to be insufficient.

IV. TOMOGRAPHIC INVERSIONS USING PRIOR INFORMATION

In order to determine the effect of the presented inversion methods on the scarce two-view FIDA signal, the fast-ion distribution before the sawtooth crash is reconstructed from a synthetic signal with added noise generated using TRANSP (Figure 3a).

Figure 5 shows the resulting reconstructions. Panels (a) and (b) shows high-definition inversions as applied in previous work[13,22]. Panels (c) and (d) show high-definition inversions using our new method where we identify the unlikely velocity-space before the inversion according to Eq. (4). The distribution in panel (c) is inferred from the unlikely velocity-space method above the neoclassically expected limit, whilst panel (d) gives the solution from the unlikely velocity-space method on
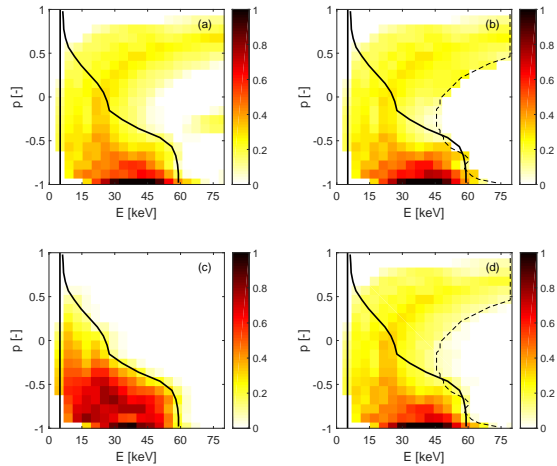
FIG. 5. Inversion of the synthetic signal generated from the TRANSP simulation for before the sawtooth crash. Each panel uses different prior information: (a) non-negativity, (b) non-negativity and null-measurement constraint, (c) the unlikely velocity-space method above what is neoclassically expected, and (d) the unlikely velocity-space method in the null-measurement region, with $\lambda_1 = 5 \times 10^9$ and $\lambda_0 = 1$. All plots are normalized by the same factor as in Figure 3.

the null-measurement region as an alternative to the hard null-measurement constraint.

Using only the non-negativity constraint (Figure 5a), the solution is plagued by high densities within two parabola-shaped bands at energies above what is neoclassically expected. Since we are here reconstructing based on synthetic measurements, we know the true solution (Figure 3a), and we know that these bands are artifacts. These artificial bands follow the outer edge of the interrogation regions of the two views (see Figure 2) and are partially caused by the lack of toroidal weight function coverage in the positive pitch-range. Including the hard null-measurement constraint in the reconstruction (Figure 5b) improves the solution for negative pitches, where the null-measurement region nearly limits the solution to the upper boundary of the TRANSP simulation. However, since only the redshifted part of the toroidal view is accessible, no null-measurements are available to prove that the positive-pitch band is an artifact. In addition, the null-measurement constraint introduces a sharp boundary between the null-measurement region and the available velocity-space. This sharp boundary is replaced by a smoother decay when replacing the hard null-measurement constraint (Figure 5b) with the exponentially growing penalty term in the null-measurement region in panel (d). The removal of the sharp boundary is most clear near 60 keV at pitches below −0.5. Hence, substituting the hard null-measurement constraint with the unlikely velocity-space method in the null-measurement region will likely prove favourable in tomography problems in the future. How-

ever, here this method does not remove the prominent artificial band at positive pitches. Using instead the unlikely velocity-space method derived from the TRANSP simulation, the artificial band at positive pitches is additionally suppressed and the solution is strongly improved over the entire domain. The suppression of densities in the unlikely velocity-space additionally leads to elevated densities in the neoclassically expected densely populated region of velocity-space which improves the match with TRANSP also in this region.

We conclude that the unlikely velocity-space method assuming low probabilities of fast-ion densities above what is neoclassically expected overcomes some of the encountered problems in previously suggested methods for fast-ion tomography from scarce datasets. This enables the study of the impact of a sawtooth on the fast-ion distribution from the dual-view FIDA diagnostic at MAST in the following section.

V. THE FAST-ION DISTRIBUTION BEFORE AND AFTER A SAWTOOTH CRASH

Here we study the effect of the sawtooth crash on the fast-ion density using both the FIDASIM simulations and the measured signals presented in Figure 1. The fast-ion density is obtained by integration of the velocity distribution function[11]. The measurements lie significantly below the simulation which is probably in part explained by a calibration error. Therefore, we here make no statement about the absolute fast-ion density, but focus on the relative sawtooth crash size, which is not affected by the scaling as it is the same before and after the crash.

Figure 6 shows the reconstructions of the fast-ion distributions from the noisy FIDASIM simulations (panels (a)-(b)) and the reconstructions from measurements (panels (c)-(d)) before and after the sawtooth crash. Here we use the unlikely velocity-space method assuming only a small likelihood of ions possessing energies and pitches above the expected limit in the neoclassical TRANSP simulations. The generally lower fast-ion densities in the reconstructions from the measurements compared to the densities obtained from the FIDASIM reconstructions are explained by the lower radiance detected in the experimental signals compared to what was expected by FIDASIM (see Figure 1) which is probably related to the uncertain calibration mentioned above.

We focus on the fastest ions above 30 keV as the toroidal view does not cover lower energies. Here the TRANSP simulation predicts a fast-ion density decrease of 48%. In the reconstructions from the FIDASIM and experimental signals, the corresponding fast-ion density decreases are 46% and 42%, respectively. At ASDEX Upgrade, the measured decrease of the fast-ion density by velocity-space tomography was also smaller than in a corresponding TRANSP simulation[13].

The slightly smaller relative fast-ion density decrease in the reconstructions from the measurements, compared
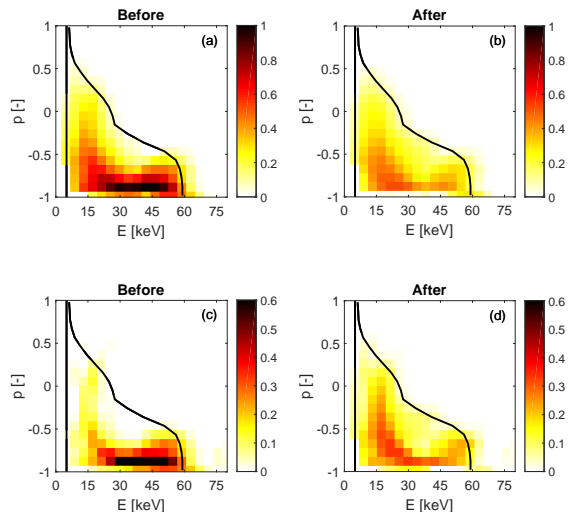
FIG. 6. Reconstructions of the FIDASIM (a)-(b) and experimental (c)-(d) signals before and after the sawtooth crash using $\lambda_1 = 5 \times 10^9$ and $\lambda_0 = 1$. All plots are normalized by the same factor as in Figure 3.

to the density decrease obtained from the FIDASIM signals, originates partly from the vertical view measurements that stay approximately constant over the sawtooth crash. This is supported by observations on reconstructions using only one view: Removing the vertical view in the reconstructions from the experimental signal results in a density decrease of more than 50%, whilst a reconstruction using only the vertical view yields no significant change in density. This agrees with observations from other machines where sawtooth crashes most strongly affect passing fast ions[12].

VI. CONCLUSION

We studied velocity-space tomography based on the dual-view FIDA measurements at MAST which constitutes a scarce-data problem. For this type of scarce-data problem, the use of prior information is essential to obtain usable inversions. However, reconstructions of the fast-ion velocity distribution using only previously introduced tomographic methods are plagued by clearly artificial increased-density structures at positive pitches covered by only the vertical view. To overcome this, we introduce a new way of including prior information. We identify the portion of velocity-space that is unlikely to have significant fast-ion densities. We then impose an exponentially growing penalty function in the unlikely velocity-space. Ideally, this region should be determined solely by null-measurements, which proves to be an advantageous alternative to the hard null-measurement constraint that is being used in high-definition tomog-

raphy. However, in this study the null-measurement penalty method does not suppress all clear artifacts. We therefore propose to use the neoclassical TRANSP simulation to determine the unlikely velocity-space by assuming it unlikely that ions possess energies and pitches far above what is neoclassically expected. This additional prior information results in a strongly improved solution. Using this method, the fast-ion velocity distributions before and after a sawtooth crash have been reconstructed from experimental measurements for energies above 30 keV. The relative decrease in the fast-ion density over the sawtooth crash is marginally smaller than in the TRANSP simulation as was also found at ASDEX Upgrade.

[1]S. D. Pinches et al., Plasma Phys. Control. Fusion 46, B187 (2004).
[2]W. W. Heidbrink, Rev. Sci. Instrum. 81, 10D727 (2010).
[3]W. W. Heidbrink et al., Plasma Phys. and Control. Fusion 46, 1855 (2004).
[4]J. Huang et al., Rev. Sci. Instrum. 87, 11E542 (2016).
[5]T. Ito et al., Rev. Sci. Instrum. 81, 10D327 (2010).
[6]M. Podestá et al., Rev. Sci. Instrum. 79, 10E521 (2008).
[7]M. Weiland et al., Plasma Phys. and Control. Fusion 58, 025012 (2016).
[8]B. Geiger et al., Plasma Phys. and Control. Fusion 59, 115002 (2017).
[9]C. A. Michael et al., Plasma Phys. Control. Fusion 55, 095007 (2013).
[10]M. Cecconello et al., Plasma Phys. and Control. Fusion 57, 014006 (2015).
[11]B. Geiger et al., Nucl. Fusion 55, 083001 (2015).
[12]A. S. Jacobsen et al., Plasma Phys. Control. Fusion 58, 042002 (2016).
[13]M. Salewski et al., Nucl. Fusion 56, 106024 (2016).
[14]A. Kirk et al., Nucl. Fusion 57, 102007 (2017).
[15]W. W. Heidbrink et al., Com. Comput. Phys. 10, 716741 (2011).
[16]A. Pankin et al., Comput. Phys. Commun. 159, 157 (2004).
[17]M. Salewski et al., Plasma Phys. Control. Fusion 56, 105005 (2014).
[18]M. Salewski et al., Nucl. Fusion 52, 103008 (2012).
[19]M. Salewski et al., Nucl. Fusion 54, 023005 (2014).
[20]M. Salewski et al., Nucl. Fusion 53, 063019 (2013).
[21]P. C. Hansen, Discrete Inverse Problems: Insight and Algorithms (SIAM, 2010).
[22]M. Salewski et al., Nucl. Fusion 57, 056001 (2017).
[23]M. Weiland et al., Nucl. Fusion 57, 116058 (2017).